2008

Fabrication of Well-Defined Block Copolymer Nano-Cylinders by Controlling the Thermodynamics and Kinetics Involved in Block Copolymer Self-Assembly

Dae Up Ahn, *University of Akron Main Campus*
Erol Sancaktar, *University of Akron*

Fabrication of well-defined block copolymer nano-cylinders by controlling the thermodynamics and kinetics involved in block copolymer self-assembly†

Dae Up Ahn and Erol Sancaktar*

Received 28th January 2008, Accepted 25th March 2008
First published as an Advance Article on the web 1st May 2008
DOI: 10.1039/b801515e

Self-assembled 3-dimensional perpendicular cylinder orientation was achieved mainly by thermodynamic control of incompatibility between the block domains, and further precise modification of size and hexagonal alignment of perpendicular cylinders was also accomplished by kinetic control of diffusive molecular mobility of block copolymer microdomains. Since those two controls have been achieved by simple blending of minority homopolymers, the intrinsic advantages of block copolymer nanopatterning, such as fast and spontaneous 3-dimensional nanopatterning with high stability and reproducibility, have been completely preserved in this fabrication strategy. Thus, the fabrication strategy using the simple blending of a block copolymer with its homopolymer at an appropriate molecular weight creates new opportunities for the fabrication of low-cost and high-throughput nanostructured block copolymer materials with highly controlled 3-dimensional nanopatterns.

I. Introduction

During the past decades, block copolymers possessing chemically different block components, which spontaneously self-assemble into ordered nanostructures due to their covalent bonding, have attracted great attention for their nanotechnological application potential.[1–3] On the other hand, commercial applications of such block copolymers have been restricted due to the difficulties in controlling the order of block copolymer nanopatterns throughout the whole sample thickness and area.[3] Consequently, external fields and treatments, such as mechanical flow fields, electrical fields, neutral substrates and solvent annealing methods have been applied during their self-assembly processes to produce a long-range order of block copolymer nanostructure.[4–7] However, such external field application techniques did not successfully provide long-range periodic ordered block copolymer nanopatterns along the substrate x,y-plane without a sample thickness constraint.[8–10] As an alternative internal technique, the blending of a block copolymer with its majority and/or minority homopolymer has recently attracted a great deal of nanotechnological interest since the 2- and 3-dimensional nanopatterns in the block copolymers can be readily modified by the addition of homopolymer with an appropriate molecular weight.[9–15] In addition to the size and periodic spacing of a block copolymer nanopattern, its long-range order and 3-dimensional orientation were also manipulated by controlling the amount and/or the molecular weight of a blended homopolymer. Thus, such block copolymer–homopolymer mixtures have been expected to be used as nano-porous materials with well-defined pore sizes, photonic materials for selective filtering of certain wavelengths of light, and nanotemplates for the fabrication of nanometre-scale topographic patterns on inorganic substrates.[9,10]

The phase behavior of a block copolymer–homopolymer mixture is primarily governed by the relative length of the homopolymer chain in comparison to that of its counterpart block component in the block copolymer at a fixed amount of blended homopolymer.[10–14,16] Three different phase behaviors have been experimentally identified, depending on the degree of polymerization of homopolymer A, N_{AH}, and that of its corresponding block component in the block copolymer, N_{AC}.[14,16] If $N_{AH} < N_{AC}$, the homopolymer A tends to be selectively solubilized into an A microdomain, which leads to a swelling of the A domain, and hence it causes a change in the overall domain spacing and morphology of the neat block copolymer. When $N_{AH} \approx N_{AC}$, the homopolymer A has much more tendency to be localized at the center of the A microdomains, and consequently it does not notably induce a swelling of the A domain. If $N_{AH} > N_{AC}$, the phase changes of a block copolymer–homopolymer mixture are influenced by the macrophase separation between the block copolymer and the homopolymer as well as the microphase separation between the block components.

However, we note that such classification was mainly concerned with the entropic contribution of blended homopolymer even though its enthalpic and kinetic contributions would also be remarkably involved in the process of homopolymer-driven block copolymer microphase transition. Since the degree of incompatibility between the block domains will be significantly modified by the addition of corresponding homopolymers, the enthalpic contribution of blended homopolymer should be considered to illustrate such homopolymer-driven microphase transition phenomena. Furthermore, the kinetic contribution of blended homopolymer cannot be neglected when we describe the changes in the block copolymer nanostructure after the blending with homopolymer of different molecular weights because the molecular weight of the blended homopolymer will also considerably influence the diffusion rate of the block copolymer microdomains.

Department of Polymer Engineering, The University of Akron, Akron, OH 44325-0301, U. S. A. E-mail: erol@uakron.edu; Fax: (+330) 258-2339; Tel: (+330) 972-5508

† Electronic supplementary information (ESI) available: Further details on the thermodynamic and kinetic stability of the block copolymers used, and the perpendicular cylinder orientation of the block copolymer mixtures throughout the whole sample thickness. See DOI: 10.1039/b801515e

In this study, we investigated the changes in microdomain structure of a cylinder-forming block copolymer upon incorporation of its minority homopolymers with different molecular weights. Based on the experimental results providing size-tunable block copolymer nano-cylinders with perpendicular and hexagonal alignments on a preferential substrate, we illustrated that the enthalpic and kinetic contributions of blended homopolymer dominantly governed the phase behaviors and phase transitions of block copolymer–homopolymer mixtures.

II. Materials and experiments

As a standard material composed of parallel cylinders, a commercial grade of polystyrene-*block*-polyisoprene-*block*-polystyrene (SIS, Vector 4113, DEXCO Polymers Co.) triblock copolymer was used as received. This triblock copolymer is highly asymmetric in block composition, and contains 15.4 wt% of polystyrene (PS). Five PSs with different molecular weights were synthesized by anionic polymerization using *sec*-butyllithium as an initiator, benzene as a solvent, and standard high-vacuum techniques: PS4k (the weight average molecular weight, M_w = 4.0 kg mol^{-1} and polydispersity index, PDI = 1.09), PS12k (M_w = 12.2 kg mol^{-1} and PDI = 1.08), PS15k (M_w = 15.4 kg mol^{-1} and PDI = 1.03), PS27k (M_w = 26.7 kg mol^{-1} and PDI = 1.03), and PS43k (M_w = 43.2 kg mol^{-1} and PDI = 1.03). The M_w and the PDI (M_w/M_n) of SIS triblock copolymer and PS homopolymers were determined from the gel permeation chromatography (GPC, Waters) data based on the calibration with a PS standard of known molecular weight and PDI. The PS weight percent of the block copolymer was determined by proton nuclear magnetic resonance (^{1}H-NMR, Varian VXR 200) spectroscopy.

Predetermined amounts of neat SIS triblock copolymer or its blends with PS homopolymers were dissolved in toluene (3.5 wt% in solution for ~100 nm thick films) with 0.05 wt% of antioxidant (Irganox 1010, Ciba-Geigy Group). Thin film samples with ~100 nm thickness were spin-coated from the solution onto silicon wafers (they were first treated with piranha solution, a 70 : 30 solution of concentrated sulfuric acid and 30% hydrogen peroxide, at 60 °C and then treated with 48% hydrofluoric acid, HF, at ambient temperature) at 2000 rpm. Thicker film samples (300–500 nm, ~10 μm and ~100 μm thick samples) were prepared by solution casting onto poly(tetrafluoroethylene) (Teflon), polyimide (Kapton), and poly(ethylene terephthalate) (PET, Mylar) substrates. The solvent of the solution-cast samples was slowly evaporated under ambient conditions for 2 d and then in a vacuum oven at 50 °C for a day. Finally, all the samples were annealed in a vacuum oven at different annealing temperatures, which were well above the glass transition temperatures of PS block and PS homopolymers. Six different samples were prepared and they were individually denoted: (1) neat SIS, (2) SIS + PS4k (90 wt% of neat SIS triblock copolymer and 10 wt% of PS4k), (3) SIS + PS12k (90 wt% of neat SIS triblock copolymer and 10 wt% of PS12k), (4) SIS + PS15k (90 wt% of neat SIS triblock copolymer and 10 wt% of PS15k), (5) SIS + PS27k (90 wt% of neat SIS triblock copolymer and 10 wt% of PS27k), and (6) SIS + PS43k (90 wt% of neat SIS triblock copolymer and 10 wt% of PS43k). It is notable that further increase in the PS homopolymer molecular weight above 27 kg mol^{-1} did not produce miscible blends at the microscopic level of film thickness due to the partial macrophase separation between the SIS triblock copolymer and PS homopolymer. In addition, nine different SIS triblock copolymer–PS homopolymer blends containing two different PS homopolymers were prepared: (1) SIS + PS4k13 + PS27k1 (blend of 90 wt% of SIS triblock copolymer, 9.3 wt% of PS4k and 0.7 wt% of PS27k, the M_w of the two PSs ≈ 12 kg mol^{-1}), (2) SIS + PS4k7 + PS27k1 (blend of 90 wt% of SIS triblock copolymer, 8.8 wt% of PS4k and 1.2 wt% of PS27k; the M_w of the two PSs ≈ 15 kg mol^{-1}), (3) SIS + PS12k5 + PS15k5 (blend of 90 wt% of SIS triblock copolymer, 5 wt% of PS12k and 5 wt% of PS15k), (4) SIS + PS12k7 + PS15k3 (blend of 90 wt% of SIS triblock copolymer, 7 wt% of PS12k and 3 wt% of PS15k); (5) SIS + PS12k9 + PS15k1 (blend of 90 wt% of SIS triblock copolymer, 9 wt% of PS12k and 1 wt% of PS15k); (6) SIS + PS12k5 + PS27k5 (blend of 90 wt% of SIS triblock copolymer, 5 wt% of PS12k and 5 wt% of PS27k); (7) SIS + PS12k7 + PS27k3 (blend of 90 wt% of SIS triblock copolymer, 7 wt% of PS12k and 3 wt% of PS27k); (8) SIS + PS12k8 + PS27k2 (blend of 90 wt% of SIS triblock copolymer, 8 wt% of PS12k and 2 wt% of PS27k); and (9) SIS + PS12k9 + PS27k1 (blend of 90 wt% of SIS triblock copolymer, 9 wt% of PS12k and 1 wt% of PS27k).

The annealing-temperature dependent block copolymer morphologies were identified with a Nanoscope III from Digital Instruments. The atomic force microscopy (AFM) was conducted in the tapping mode under ambient conditions using commercial silicon microcantilever probe tips (Veeco, RTESP5) with spring constants ranging from 20 to 80 N m^{-1} as specified by the manufacturer. The thermal histories of the block copolymer samples used in AFM measurements were controlled so that they would be similar to those experienced in dynamic mechanical measurements.

The dynamic mechanical properties of the SIS triblock copolymer and its mixtures were measured with an Advanced Rheometric Expansion System (ARES, Rheometric Scientific). The measurements were conducted in shear oscillatory mode using a 25 mm diameter parallel disk geometry with a gap setting of ~2 mm. In order to prepare ~2 mm thick samples for dynamic mechanical measurements, the ~10 μm thick samples solution-cast onto Teflon substrates were stacked layer-by-layer, and then they were gently pressed at ~100 °C. The block copolymer samples were annealed at a selected temperature for 10 min before starting dynamic mechanical measurements, and all data were collected for ~20 min each per selected temperature under a nitrogen atmosphere to prevent thermal degradation of the samples. The range of angular frequency (ω) was from 0.05 to 100 rad s^{-1} and the range of temperature was selected from 110 °C to 250 °C, depending on the sample. The strain amplitude of 2% was selected to be large enough for accurate torque signals, small enough to keep the material response in the linear region, and sufficiently minimal enough to neglect shear effects on microphase phase separation processes of block copolymer mixtures.

III. Results and discussion

A. Block copolymer cylinder orientation transition by blending minority homopolymers with different molecular weights

Fig. 1 shows AFM images of SIS triblock copolymer and its miscible homopolymer mixtures annealed on Teflon substrates at 130 °C for 50 h. Since the volume fractions of PS correspond to

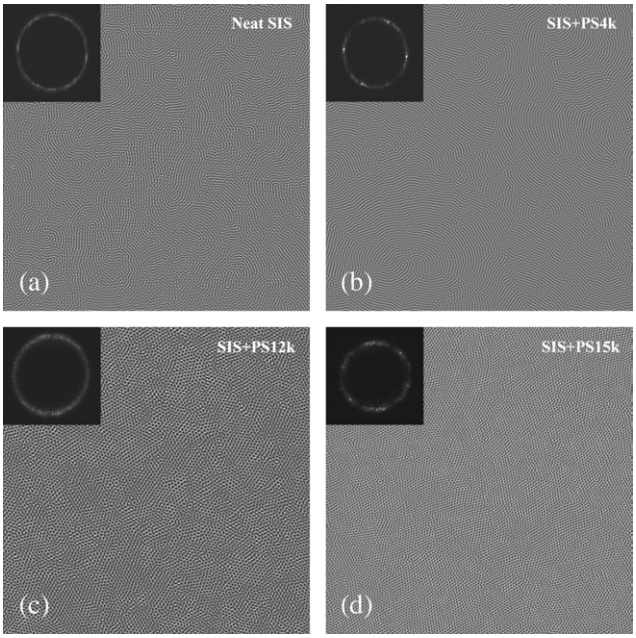

Fig. 1 AFM images of neat SIS and its miscible PS homopolymer mixtures at different homopolymer molecular weights. Images were obtained from ~10 μm thick samples annealed at 130 °C on the Teflon substrates. Topographic and phase images were the same. Inset is a 2D FFT of the image. The images show an area of 5 × 5 μm^2.

the cylindrical array (~13 vol% of PS in neat SIS triblock copolymer and 20–22 vol% of PS in block copolymer mixtures at the annealing temperature), the images represent cylinders parallel or perpendicular to the surface. It is notable that the cylinder orientation of miscible block copolymers spin-coated on HF-treated silicon wafer (thickness ≈ 100 nm) was identical to that of the block copolymers solution-cast on Teflon substrates in the range of film thickness from ~500 nm to ~10 μm. Furthermore, the bottom surface cylinder orientation of each sample deposited on Teflon substrates was not much different from its top orientation. Thus, the thickness parameter in neat SIS and its miscible homopolymer blends does not significantly affect their cylinder orientation in the range of sample thickness from the sample–substrate interface to ~10 μm, even though they are deposited on preferential fluorine substrates (*i.e.*, HF-treated and Teflon substrates).[10]

In comparison to the undulated parallel cylinders in neat SIS, relatively more straightened parallel cylinders were observed in SIS + PS4k (the molecular weight ratio between the PS homopolymer and its corresponding PS block, *i.e.*, higher molecular weight PS component/lower molecular weight PS component, $r = 3.6$.) on the fluorine substrates, as shown in Fig. 1 (a) and (b). The 2D fast Fourier transforms (FFTs) included as insets in Fig. 1 also clearly demonstrate that the straightness of the parallel cylinders in the x,y-plane is enhanced by the addition of PS4k. On the preferential fluorine substrates, on the other hand, perpendicularly oriented and hexagonally packed block copolymer cylinders were spontaneously produced in SIS + PS12k (r = 1.2) and SIS + PS15k ($r = 1.1$) throughout the whole sample area without any external field application [Fig. 1 (c) and (d)]. It is notable that the size and periodicity of the perpendicular

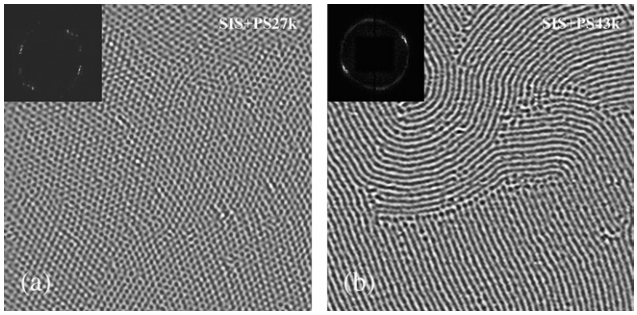

Fig. 2 AFM images of partially miscible SIS triblock copolymer mixtures at different homopolymer molecular weights. Images were obtained from ~500 nm thick samples annealed at 130 °C on the Teflon substrates. Topographic and phase images were the same. The inset is a 2D FFT of the image. The images show an area of 2 × 2 μm^2.

cylinders decrease as the molecular weight of the blended homopolymer increases, *i.e.*, the average diameter of the perpendicular cylinders is ~38 nm and the average center-to-center spacing between the nearest perpendicular cylinders is ~75 nm for SIS + PS12k, and the diameter is ~28 nm and the center-to-center spacing is ~55 nm for SIS + PS15k. In addition, it can also be confirmed from the comparison of the 2D FFTs of images in Fig. 1 (c) and (d) that the hexagonal ordering of perpendicular cylinders is enhanced with the increase in blended PS homopolymer molecular weight.

Fig. 2 shows AFM images of partially immiscible SIS triblock copolymer mixtures, SIS + PS27k ($r = 1.9$) and SIS + PS43k (r = 3.0). We note that their overall uniform morphologies were observed only in the thickness range from the sample–substrate interface to ~500 nm because of the macrophase separation between the neat SIS and the high molecular weight homopolymers (*i.e.*, PS27k and PS43k), as well as the microphase separation between the PI and PS components, above the ~500 nm sample thickness. In the ~500 nm thick samples, the SIS + PS27k displayed a long-range perpendicular cylinder orientation in the x,y-plane, while the SIS + PS43k showed a majority of parallel orientation over a wide sample area. The average diameter of the perpendicular cylinders in SIS + PS27k was ~22 nm and their average center-to-center spacing was ~44 nm.

B. Temperature-dependent phase behavior of block copolymer mixtures

The AFM images Fig. 3 show the temperature-dependent microphases of neat SIS and its PS homopolymer blends. In cases of parallel cylinder-forming neat SIS and SIS + PS4k, the straightness of the parallel cylinders was gradually enhanced with increasing temperature. In comparison, perpendicular cylinder-forming SIS + PS12k showed a gradual orientation transition from perpendicular to parallel with increasing temperature in the temperature range from 130 °C to 210 °C. Consequently, the overall perpendicular cylinder orientation of SIS + PS12k at 130 °C was thoroughly transferred to parallel cylinder orientation at 210 °C. In the case of SIS + PS15k, more stable perpendicular cylinders were observed at temperatures ranging from 130 °C to 150 °C, and then hexagonal lattice disordering of perpendicular cylinders was identified in the

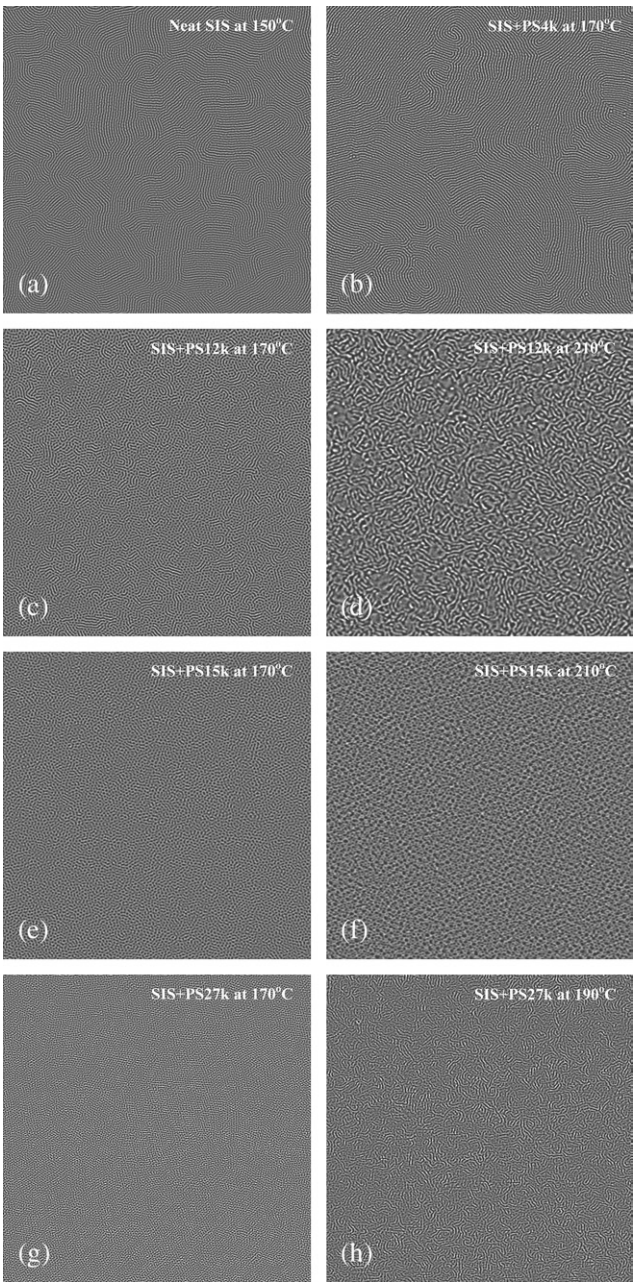

Fig. 3 Temperature-dependent phase behaviors of neat SIS and its PS homopolymer mixtures. AFM images of neat SIS, SIS + PS4k, SIS + PS12k and SIS + PS15k were obtained from ~10 μm thick samples annealed on the Teflon substrates, and those of SIS + PS27k were obtained from ~500 nm thick samples annealed on the Teflon substrates.[31] The images show an area of 5 × 5 μm^2.

temperature range between 170 °C and 210 °C. During the disordering process, the perpendicular cylinders in SIS + PS15k merged together to decrease the interfacial area between the PS and polyisoprene (PI) domains without a perpendicular to parallel cylinder orientation transition. Similar to the case of SIS + PS12k, SIS + PS27k also showed a gradual orientation transition from perpendicular to parallel as the annealing temperature increased in the temperature range from 130 °C to 190 °C, and consequently lost its perpendicular cylinder orientation at ~200 °C. Thus, we realize that the preference for perpendicular orientation in SIS + PS15k is exceptionally stronger than in SIS + PS12k and SIS + PS27k. We note that the parallel cylinder orientation of neat SIS is spontaneously transferred to a perpendicular one as the molecular weight ratio between the homologous PS pair approaches unity as long as the ratio is approximately larger than 1.1, and such orientation transition corresponds to the temperature-dependent phase behavior of SIS + PS12k, which presumably occurs by lowering the annealing temperature. Therefore, we realize that the thermodynamic driving forces involved in temperature-dependent phase behavior are nearly equivalent to those involved in the homopolymer molecular weight dependent phase transition.

C. Theoretical consideration of parallel to perpendicular cylinder orientation transition: interaction force between a homologous polymer pair

We note that the homopolymer- and/or temperature-driven parallel to perpendicular cylinder orientation transition does not significantly originate from the compositional variation of a block component because the amount of incorporated PS homopolymer is fixed at 10 wt% in all five block copolymer mixtures. Thus, we tentatively assume that the incompatibility between the block domains, denoted χN (where χ is the Flory–Huggins segmental interaction parameter and N is the degree of polymerization), would induce such a cylinder orientation transition. If we assume that the contributions of the homologous PS pair (*i.e.*, PS homopolymer and its corresponding PS block in SIS) to the domain–domain incompatibility routinely depend on their average molecular weight, the χN values can be calculated as 61, 59, 61, 62, 65 and 68 for neat SIS, SIS + PS4k, SIS + PS12k, SIS + PS15k, SIS + PS27k and SIS + PS43k, respectively, at an annealing temperature of 130 °C.[17] Such mutually similar χN values, however, neither provide a critical explanation of the homopolymer-driven cylinder orientation transition phenomenon nor reasonably explain the different temperature-dependent phase behaviors of perpendicular cylinder-forming block copolymers. Note that the perpendicular cylinder orientation was not obtained when the molecular weight of the blended homopolymer (*i.e.*, the incompatibility between the block domains) routinely increased; rather it was achieved when the molecular weight ratio between the homologous PS pair approached unity as long as it is approximately larger than 1.1. Furthermore, the exceptionally strong preference for perpendicular cylinder orientation in SIS + PS15k cannot be described by its χN value being nearly identical to that of SIS + PS12k. Therefore, we provide an alternative thermodynamic consideration for the block copolymer orientation transition phenomena at a fixed composition.

If we consider a parallel to perpendicular cylinder orientation transition at a fixed total sample volume and volume fraction of the minority block component (Fig. 4), the ratio between the perpendicular and parallel domain–domain excess free energies (G/G_0) is given by:

$$\frac{G}{G_0} = \frac{\gamma(M_w, T)A}{\gamma_0(M_{w,0}, T)A_0} = \frac{\gamma 2\pi rtN}{\gamma_0 2\pi r_0 LN_0} = \frac{\gamma r_0}{\gamma_0 r} \quad (1)$$

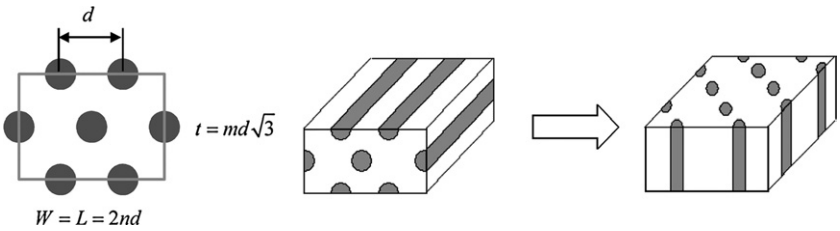

Fig. 4 Simple model for the cylinder orientation conversion from parallel to perpendicular: d is the center-to-center spacing between the parallel cylinders, t is the sample thickness, m and n are the multiplying factors ($n \geq m$), W is the sample width, L is the sample length, r_0 is the radius of the initial parallel cylinders, r is the radius of the perpendicular cylinders, N_0 is the number of initial parallel cylinders, and N is the number of perpendicular cylinders.

Here, A/A_0 is the ratio between the perpendicular and parallel domain–domain interfacial areas and γ is the interfacial energy between the block components, depending on the average molecular weights of the block components and the annealing temperature, T. In addition, the ratio of the interfacial area between the minority domain and the substrates (or superstrates) ($A_{\text{minor}}/A_{\text{minor},0}$) and its corresponding ratio of excess free energy ($G_{\text{minor}}/G_{\text{minor},0}$) are given by:

$$\frac{G_{\text{minor}}}{G_{\text{minor},0}} \approx \frac{A_{\text{minor}}}{A_{\text{minor},0}} = \frac{2\pi r^2 N}{2r_0 2nd4n} = \frac{\pi r_0}{d\sqrt{3}} = a \qquad (2)$$

The ratio of the interfacial area between the majority domain and the substrates (or superstrates) ($A_{\text{major}}/A_{\text{major},0}$) and its corresponding ratio of excess free energy ($G_{\text{major}}/G_{\text{major},0}$) are also given by:

$$\frac{G_{\text{major}}}{G_{\text{major},0}} = \frac{A_{\text{major}}}{A_{\text{major},0}} = \frac{2\left(4n^2d^2 - \frac{4n^2 2\pi r_0}{d\sqrt{3}} r_0 d\right)}{2(4n^2d^2 - 8n^2 r_0 d)} = \frac{d - 2ar_0}{d - 2r_0} \qquad (3)$$

For parallel cylinder orientation, the fractions of interfacial areas, f_0s are given by:

$$\begin{aligned} f_{\text{domain-domain},0} &= \frac{A_0}{A_{\text{total},0}} = \frac{2m\pi r_0}{d + 2m\pi r_0} \\ f_{\text{major-substrate},0} &= \frac{A_{\text{major},0}}{A_{\text{total},0}} = \frac{d - 2r_0}{d + 2m\pi r_0} \\ f_{\text{minor-substrate},0} &= \frac{A_{\text{minor},0}}{A_{\text{total},0}} = \frac{2r_0}{d + 2m\pi r_0} \end{aligned} \qquad (4)$$

Here, $A_{\text{total},0}$ is the total interfacial area of parallel cylinder-forming sample (*i.e.*, $A_{\text{total},0} = A_0 + A_{\text{major},0} + A_{\text{minor},0}$). In addition, for perpendicular cylinder orientation, the fractions of interfacial areas, fs are given by:

$$\begin{aligned} f_{\text{domain-domain}} &= \frac{A}{A_{\text{total}}} = \frac{2m\pi r_0\left(\frac{r_0}{r}\right)}{d + 2m\pi r_0\left(\frac{r_0}{r}\right)} \\ f_{\text{major-substrate}} &= \frac{A_{\text{major}}}{A_{\text{total}}} = \frac{d - 2ar_0}{d + 2m\pi r_0\left(\frac{r_0}{r}\right)} \\ f_{\text{minor-substrate}} &= \frac{A_{\text{minor}}}{A_{\text{total}}} = \frac{2ar_0}{d + 2m\pi r_0\left(\frac{r_0}{r}\right)} \end{aligned} \qquad (5)$$

Here, A_{total} is the total interfacial area of perpendicular cylinder-forming sample.

Using experimentally determined cylinder dimensions and the above equations, we can estimate the relative interfacial area changes after the orientation conversion process from parallel to perpendicular. It is notable that, in order to estimate the above equations, we do not need to consider any types of thermodynamic driving forces involved in the cylinder orientation transition because we use the experimentally (*i.e.*, thermodynamically and kinetically) already determined cylinder dimensions to calculate the changes in interfacial areas and excess free energies due to the geometric orientation transition from parallel to perpendicular.[18] During the calculation, in order to represent the interfacial areas and energies of perpendicular cylinders, we designated the dimensional characteristics of SIS + PS4k as reference dimensional values of parallel cylinders because the PS block composition of SIS + PS4k is similar to those of SIS + PS12k, SIS + PS15k and SIS + PS27k. As shown in the third, forth and fifth columns of Table 1, the excess free energy between the block domains and that between the majority block and the substrate should be enlarged after the parallel to perpendicular orientation transition. In addition, the change in the interfacial area between the block domains will be the most critical factor for the cylinder orientation transition due to its largest fraction (see the sixth, seventh and eighth columns of Table 1). Considering the calculation results together with our experimental results, therefore, we conclude that perpendicular orientation-inducing thermodynamic conditions such as the blending of a minority homopolymer with an appropriate molecular weight and the lowering of the annealing temperature should generate a considerable amount of excess free energy into the block domains. Thus, we can expect that a strong thermodynamic compensation should be involved in the process of parallel to perpendicular cylinder orientation transition to overcome the increased domain–domain excess free energy. Note that such unfavorable cylinder orientation transition spontaneously occurred in our block copolymer mixtures.

As a strong enthalpic interaction force surpassing the increased domain–domain excess free energy, we propose an intermolecular affinity between the homopolymer and its corresponding block component, whose strength depends on the molecular weight difference between them. Our proposal implies that a homologous polymer pair with mutually different molecular weights does not recognize each different weight constituent as an identical counterpart. Thus, a thermodynamic compensation will be generated in the blend of such homologous polymer pair, whose amount is proportional to the degree of identity between them as long as their molecular weights are not exactly

Table 1 Changes in the interfacial area and excess free energy after the parallel to perpendicular cylinder orientation transition

Thickness	Sample	A/A_0 ($\gamma A/\gamma_0 A_0$)	$A_{major}/A_{major,0}$	$A_{minor}/A_{minor,0}$	$f_{domain-domain}$	$f_{majority-substrate}$	$f_{minority-substrate}$
$m = 1$	SIS + PS12k	1.0 (1.04[a])	1.56	0.46	0.61 (0.61[b])	0.30 (0.20[b])	0.09 (0.19[b])
	SIS + PS15k	1.36 (1.51[a])			0.68	0.24	0.07
	SIS + PS27k	1.73 (1.99[a])			0.73	0.20	0.06
$m = 5$	SIS + PS12k	1.0 (1.04[a])			0.89 (0.89[b])	0.09 (0.06[b])	0.03 (0.06[b])
	SIS + PS15k	1.36 (1.51[a])			0.92	0.07	0.02
	SIS + PS27k	1.73 (1.99[a])			0.93	0.05	0.02

[a] Estimated with the value of γ at 130 °C,[19] $r_0 = 19$ nm. [b] The corresponding fraction of interfacial area for SIS + PS4k.

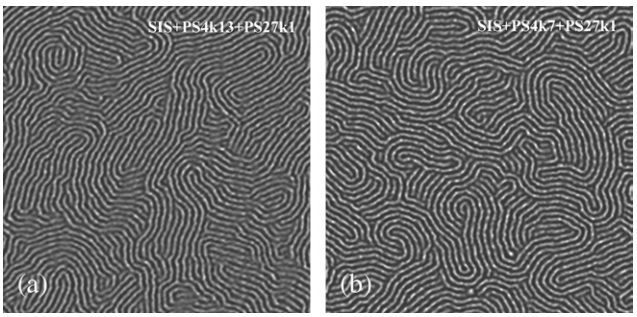

Fig. 5 AFM images of SIS + PS4k + PS27ks. Images were obtained from ~10 μm thick samples annealed at 130 °C on the Teflon substrates. Topographic and phase AFM images were the same. The images show an area of 2 × 2 μm^2.

identical. The presence of intermolecular affinity between the homologous PS pair can be confirmed more clearly from the morphological variation of neat SIS after its simultaneous blending with PS4k and PS27k (Fig. 5). Note that the blending ratio of the two PSs was controlled so that their weight average molecular weight might be similar to that of PS homopolymer, which produced a perpendicular cylinder orientation. At the same time, however, the intermolecular affinities between the PS homopolymers and their corresponding PS blocks were maintained to be negligible by selecting the homopolymer pairs to create molecular weight ratios between them and their corresponding PS blocks substantially greater than unity. Thus, a perpendicular cylinder orientation should be produced in the block copolymer mixtures of SIS + PS4k + PS27ks if the enthalpic interaction arising from the intermolecular affinity is not significantly involved in the process of homopolymer-driven orientation transition. Such a combination of homopolymer, however, did not experimentally produce a perpendicular cylinder orientation due to the significant lack of PS homopolymer molecules that enthalpically interacted with their corresponding block components. Therefore, we conclude that the homologous polymer pair interaction (*i.e.*, the enthalpic contribution of blended homopolymer) significantly influences the orientation of the block copolymer microdomains, and such interaction increases as the molecular weight ratio between the homologous PS pair approaches unity as long as their molecular weights are not exactly identical.

In the case of parallel cylinder-forming SIS + PS4k, the strength of intermolecular affinity between the homologous PS pair will be small due to their large difference in molecular weights, and hence the initial parallel cylinders in neat SIS are straightened after the blending of PS4k (or after the increase of annealing temperature) simply owing to the decreased incompatibility between the block components. On the other hand, a considerably strong intermolecular affinity between the homologous PS pair will be generated in SIS + PS12k owing to their mutually similar molecular weights. Since the strong affinity will induce an additional enhancement of incompatibility between the PS and PI components by virtue of strong segregation between the homologous PS pair, the actual incompatibility of SIS + PS12k will be much higher than the incompatibility predicted by the Flory–Huggins theory. We expect that the actual incompatibility of SIS + PS12k is ~60 at 210 °C since its undulated parallel cylinders at 210 °C are similar to those of neat SIS at 130 °C. In case of perpendicular cylinder-forming SIS + PS15k, the interaction between the homologous PS pair will further increase due to their more identical molecular weights, and hence its cylinders display an exceptionally strong preference for perpendicular orientation even at high annealing temperature (*i.e.*, even at an extremely unfavorable condition for a perpendicular cylinder orientation). The actual domain–domain incompatibility of SIS + PS15k will be much greater than ~60 at 210 °C because its perpendicular cylinder orientation is still preserved at that temperature. Similar to the case of SIS + PS12k, the actual domain–domain incompatibility of SIS + PS27k will be large enough to maintain its overall perpendicular cylinder orientation up to 170 °C, owing to the significant interaction force between the homologous PS pair. However, the perpendicular cylinder orientation of SIS + PS27k considerably disappears at 190 °C due to the relatively small contribution of homologous polymer pair interaction to the actual domain–domain incompatibility, and hence we expect that the actual incompatibility of SIS + PS27k is ~60 at ~200 °C. In the case of SIS + PS43k, such contribution of homologous PS pair interaction will further decrease due to the significant difference in molecular weight between the PS block and PS43k. Consequently, mostly parallel cylinders with a negligible amount of perpendicular cylinders were produced in the ~500 nm thick SIS + PS43k sample.

D. Interfacial interactions between the blocks and the substrates

At the minimum sample thickness ($m = 1$), we can consider another thermodynamic compensation reducing the excess free energy between the block domains that increases after the parallel to perpendicular cylinder orientation transition. As shown in the sixth, seventh and eighth columns of Table 1, the

fractional changes in the interfacial areas between each of the block domains and the substrate are not negligible at $m = 1$ after the cylinder orientation transition. In the case of thin film samples, therefore, the increased domain–domain free energy can also be relieved by reducing the excess free energy between each of the block components and the substrate, *i.e.*, (1) by enlarging the interfacial area between the substrate and its relatively favorable block component, and at the same time (2) by reducing the interfacial area between the substrate and its relatively unfavorable block component. The increased domain–domain free energy, originating from the parallel-to-perpendicular cylinder orientation transition, will be relieved on the fluorine substrates that are preferential to the PI block because the interfacial area between the fluorine substrates and their unfavorable minority PS domains will greatly decrease after achieving perpendicular cylinder orientation (see the eighth column of Table 1). Thus, a substrate that is preferential to the majority block component (at the same time, unfavorable to the minority block component) is desirable for the fabrication of perpendicular cylinders in thin films. On the other hand, a substrate that is preferential to the minority block is not suitable for the generation of a perpendicular cylinder orientation because it will not relieve the increased domain–domain excess free energy generated after the parallel to perpendicular cylinder orientation transition, but instead, it will further enhance the total excess free energy of the system together with the domain–domain excess free energy. Thus, perpendicular block copolymer cylinders in a thin film sample would partially lose their perpendicular orientation on a substrate that is preferential to the minority block if the homologous pair interaction is not strong enough to thoroughly overcome the total increase in excess free energy. As shown in Fig. 6 (a) and (b), the ~300 nm thick SIS + PS12k film sample displayed only a small amount of parallel cylinders on the polyimide and the PET substrates (unfavorable to the majority PI block, the interfacial energy between the PI and the polyimide is ~6 mJ m^{-2} and that between the PI and the PET is ~9 mJ m^{-2} at 130 °C[19]) due to its insufficient strength of homologous pair interaction, even though its complete perpendicular cylinder orientation was observed on the fluorine substrates (favorable to the majority PI block, the interfacial energy between the PI and the Teflon is ~2 mJ m^{-2} at 130 °C[19]). We note that the amount of parallel cylinders was proportional to the interfacial energy between the majority block component and the substrate, *i.e.*, a somewhat larger amount of parallel cylinders was observed on the PET substrate in comparison to the polyimide substrate. However, it is notable that the overall perpendicular cylinder orientation was still maintained in the thin film sample of SIS + PS12k on the polyimide and the PET substrates in spite of the small amount of parallel cylinders. In comparison, the cylinders in ~300 nm thick SIS + PS15k strongly maintained their perpendicular orientation on the preferential polyimide and PET substrates as well as the fluorine substrates, owing to the strong homologous PS pair interaction overwhelming the domain–substrate interfacial interactions [Fig. 6 (c) and (d)]. In the presence of a considerable intermolecular affinity between the homologous PS pair, therefore, the interfacial energy between each of the block components and the substrate will not be a significant factor for block copolymer cylinder orientation, even in thin block copolymer samples. We also note that such substrate-induced reduction of domain–domain excess free energy on the majority domain-preferential substrate becomes rapidly insignificant as the sample thickness increases. As shown in the calculation results of Table 1 at $m = 5$, the fractions of domain–substrate interfacial areas are negligible in comparison to those of domain–domain interfacial areas regardless of the block copolymer cylinder orientation. For the fabrication of perpendicular block copolymer cylinders on various preferential substrates without a significant influence of film thickness, therefore, we expect that a condition directly controlling the strength of intermolecular affinity between the block domains will be more effective than those indirectly modifying the domain–substrate interfacial energies, such as neutralization of substrate surface.[6,20]

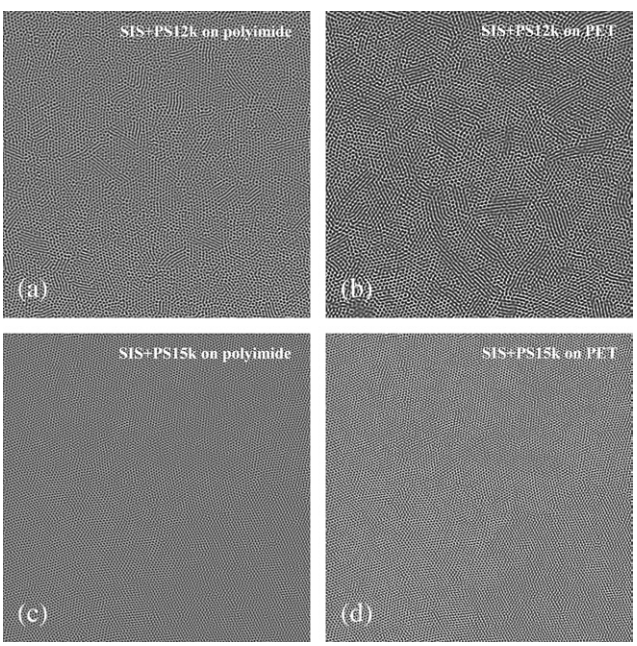

Fig. 6 AFM images of SIS + PS12k and SIS + PS15k. Images were obtained from ~300 nm thick samples annealed at 130 °C on the polyimide and PET substrates. Topographic and phase images were the same. The images show an area of 5 × 5 μm^2.

E. Thickness-dependent morphologies of cylinder-forming block copolymers

As shown in the sixth, seventh and eighth columns of Table 1, the interfacial area between the block domains (*i.e.*, the domain–domain excess free energy) will be significantly enlarged with increasing sample thickness, regardless of their preferential cylinder orientation. In order to maintain the block copolymer morphology formed in a thin film sample the intermolecular affinity between the homologous polymer pair (*i.e.*, the actual domain–domain incompatibility) should be enhanced in accordance with the thickness-proportional increase of domain–domain excess free energy. If the intermolecular affinity is not strong enough to overwhelm the thickness-proportional domain–domain excess free energy, the block copolymer mixture will have a substantial tendency to decrease the interfacial area between the block domains, proportionally enhanced with

increasing sample thickness, in order to relieve the increased domain–domain excess free energy as much as possible. As a result, the morphologies of block copolymers and their homopolymer mixtures that contain negligible or insufficient intermolecular affinity between the homologous PS pair will be significantly affected by their sample thickness.

In the case of parallel cylinder-forming block copolymers with an insignificant intermolecular affinity between the homologous PS pair, their cylinder arrays in the x,y-plane were considerably influenced by the sample thickness, even though their cylinder orientations did not vary with the sample thickness up to ~10 μm. As shown in Fig. 7 (a) and (b), the straightness of parallel cylinders in neat SIS and SIS + PS4k was enhanced with increasing sample thickness because of the thickness-proportional tendency to minimize the interfacial area between the block domains. In addition, a thickness-invariant perpendicular cylinder orientation was not observed in the ~100 μm thick SIS + PS12k and SIS + PS27k samples any more [Fig. 7 (c) and (e)] since the intermolecular affinity between the homologous PS pair was not strong enough to overcome the great amount of domain–domain excess free energy arising from the excessive increase in sample thickness. On the other hand, the SIS + PS15 still preserved its perpendicular cylinder orientation in its ~100 μm thick sample on the Teflon substrates due to the extremely strong intermolecular affinity between the PS pair (*i.e.*, actual domain–domain incompatibility), as shown in Fig. 7 (d).

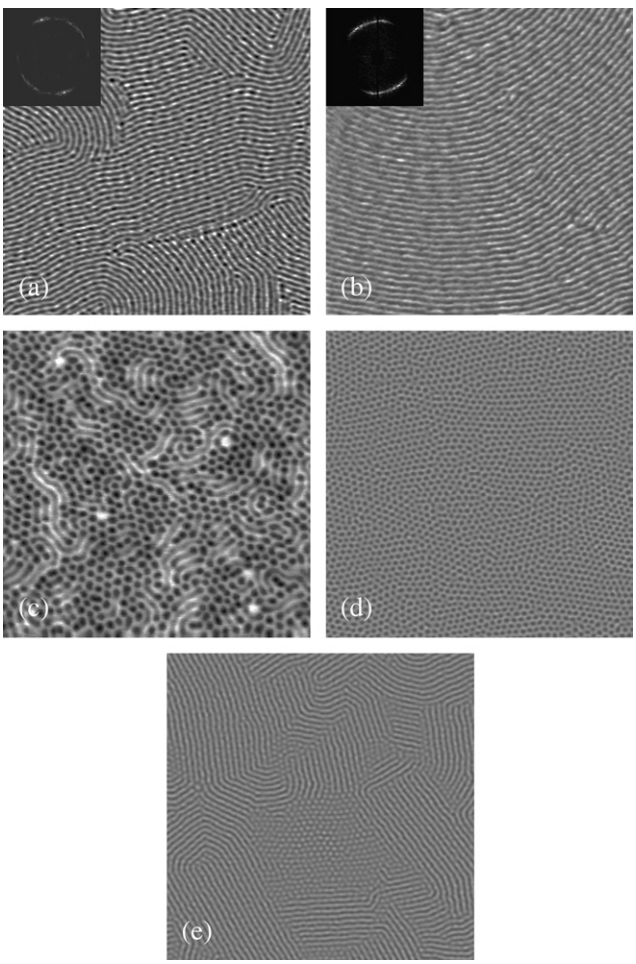

Fig. 7 AFM images of neat SIS and its PS homopolymer mixtures: (a) neat SIS, (b) SIS + PS4k, (c) SIS + PS12k, (d) SIS + PS15k, and (e) SIS + PS27k (miscible portion). Images were obtained from ~100 μm thick samples annealed at 130 °C on the Teflon substrates. Topographic and phase AFM images were the same. The inset of the AFM image is a 2D FFT of the image. The image shows an area of 2 × 2 μm².

Theoretical studies also revealed that the perpendicular cylinder orientation would be stable in thin films on a preferential substrate.[21,22] By considering the free energy difference between parallel and perpendicular cylinder orientations on a preferential substrate, it was predicted that the probability of perpendicular orientation increased as the film thickness decreased.[21] Similarly, a Monte Carlo simulation on a cylinder-forming asymmetric ABA triblock copolymer also predicted that perpendicular cylinders were stably formed in a thin film deposited on a preferential substrate over a wide-range of substrate–block interaction windows, even though the range gradually decreased with increasing film thickness.[22]

F. Heterogeneous molecular mobility in block copolymers

In the previous sections, we illustrated that perpendicularly oriented block copolymer nano-cylinders were readily achieved on a preferential substrate without any external field applications when the molecular weight ratio between the homologous PS pair approached to unity. In addition, we demonstrated that the attractive intermolecular interaction between the homologous polymer pair was a critical factor in governing the phase behaviors and phase transitions of block copolymer–homopolymer mixtures. Even though such thermodynamic considerations reasonably explain the overall homopolymer molecular weight- and temperature-dependent phase behaviors of block copolymer mixtures used, additional kinetic considerations are also required for further precise understanding of homologous polymer pair interaction-driven block copolymer phase transitions.

On the nanoscopic level, the molecular mobility of polymer molecules in the melt state can be effectively quantified with dynamic mechanical measurements since the recorded dynamic mechanical data directly represent a relaxation process of polymer melts.[23–25] It has been well known that the relaxation behavior of polymer melts follows an exponential relaxation process with a distribution of relaxation times.[24–26] Thus, the dynamic mechanical data should be treated with semi-empirical fitting functions in order to represent the relaxation behavior and determine a single average relaxation time. One of the widely accepted functions that predict such average relaxation times for polymer melts from a distribution of relaxation times is the Cole–Davidson distribution function of relaxation times.[23–25,27,28] The semi-empirical Cole–Davidson equation for a homogeneous polymer melt is given by:

$$G^*(\omega) = G_\infty \left(1 - \frac{1}{(1 + i\omega\tau_{CD})^{\beta_{CD}}}\right) \quad (6)$$

where $G^*(\omega)$ is the complex shear modulus, G_∞ is the high frequency limiting storage modulus, τ_{CD} is the maximum relaxation time present in the system, and the β_{CD} is the Cole–Davidson width parameter. In a homogeneous polymer melt system, however, the conventional Cole–Davidson equation

shows a serious fitting failure in the rubbery plateau region of polymer melts, and hence the relaxation modes of entangled polymer molecules cannot be exactly quantified by the original Cole–Davidson equation. In our block copolymer mixtures, similarly, a serious fitting failure of the original Cole–Davidson equation was also observed in the rubbery plateau-like regions, as shown in Fig. 8 (a). However, we note that such rubbery plateau-like regions of block copolymer mixtures do not originate from the molecular entanglements of the involved block components because: (1) the molecular weights of the PS domain components used in our experiment do not exceed the entanglement molecular weight (M_e) of PS where the entanglement effects start to be apparent mechanically, and (2) the temperatures applied in our experiment are too high for PI molecules to sufficiently maintain their molecular entanglements. It is notable that the M_e of PS is ~17 kg mol^{-1}, and the onset molecular weight for entanglement effects on the rheological properties of PS is approximately 2–3M_e.[29,30] Thus, we expect that such rubbery plateau-like regions observed in dynamic mechanical experiments mainly originate from the PS microdomains behaving like physical crosslinks. Using this criterion, therefore, we can divide the dynamic mechanically determined relaxation distribution of a block copolymer into two distinctive relaxation functions; one mainly originating from an elastic domain, and the other dominantly arising from a viscous domain. In other words, at a fixed temperature, the relaxation distribution observed in the rubbery plateau-like region (*i.e.*, in the low frequency region) will contain information on the average molecular mobility of PS-rich domains, and that obtained in the glass–rubber transition-like region (*i.e.*, in the high frequency region) will contain information on the average molecular mobility of PI-rich domains. According to this assumption, the original Cole–Davidson equation, which is used to obtain an average relaxation time can be modified to obtain two different average relaxation times, in the following form:

$$G^*(\omega) = G_{\infty,S}\left(1 - \frac{1}{(1 + i\omega\tau_{CD,S})^{\beta_{CD,S}}}\right) + G_{\infty,L}\left(1 - \frac{1}{(1 + i\omega\tau_{CD,L})^{\beta_{CD,L}}}\right)$$

Substitution of tanϕ for angular frequency (ω) $\times$ τ_{CD} yields

$$G'(\phi) = G^{i}_{\infty,S}[1-(\cos\phi)^{\beta}_{CD,S}\cos\beta_{CD,S}\phi] + G^{i}_{\infty,L}[1-(\cos\phi)^{\beta}_{CD,L}\cos\beta_{CD,L}\phi] \quad (7)$$

$$G''(\phi) = G^{ii}_{\infty,S}(1+(\cos\phi)^{\beta}_{CD,S}\sin\beta_{CD,S}\phi) + G^{ii}_{\infty,L}[1+(\cos\phi)^{\beta}_{CD,L}\sin\beta_{CD,L}\phi]$$

where $G^{i}_{\infty,S}$ ($G^{ii}_{\infty,S}$) and $G^{ii}_{\infty,L}$ ($G^{ii}_{\infty,L}$) are the high frequency limiting storage (loss) moduli, $\tau_{CD,S}$ and $\tau_{CD,L}$ are the Cole–Davidson relaxation times, and $\beta_{CD,S}$ and $\beta_{CD,L}$ are the Cole–

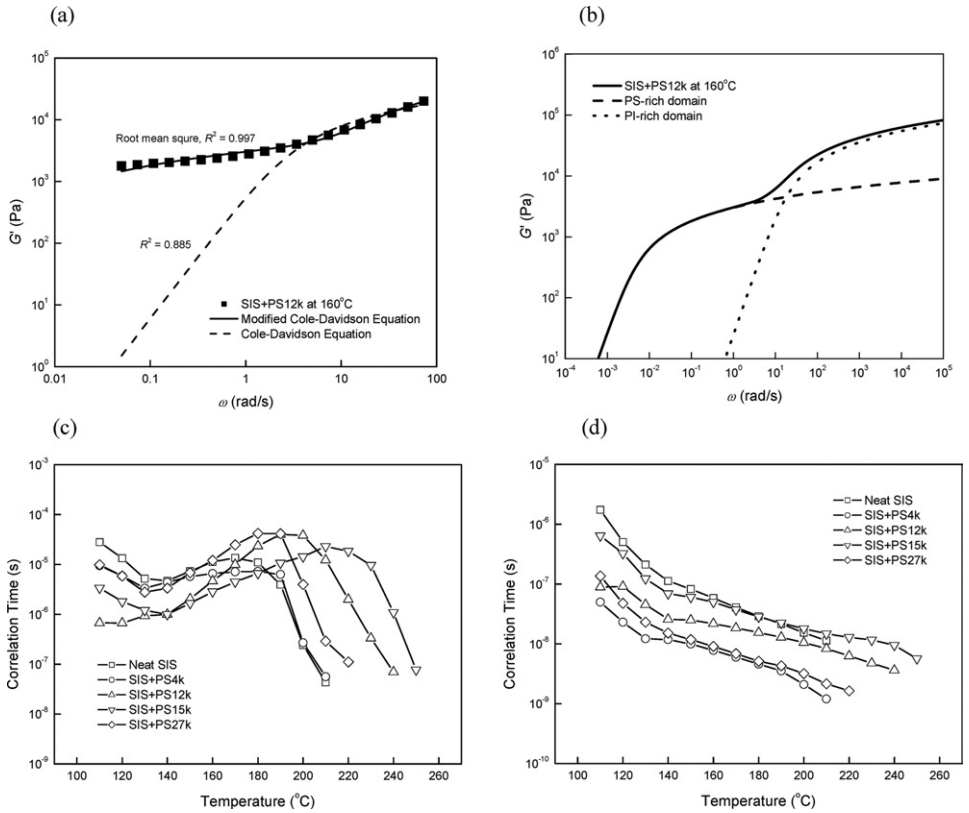

Fig. 8 Correlation times, τ_Cs, for neat SIS and its homopolymer mixtures as a function of temperature: (a) nonlinear curve fits of G' with Cole–Davidson equations; (b) identification of two different relaxation modes from the nonlinear curve fit of G' with a modified Cole–Davidson equation; (c) τ_Cs at PS-rich domain; (d) τ_Cs at PI-rich domain.

Davidson width parameters of solid-like and liquid-like domains, respectively. From nonlinear curve fittings on storage shear modulus $G'(\omega)$ and loss shear modulus $G''(\omega)$ data obtained individually at different temperatures, the temperature-dependent average relaxation time of the x domain, $\langle\tau_{CD,x}\rangle$, that is, the correlation time of the x domain, $\tau_{C,x}$, can be determined from the distribution of relaxation times as $\tau_{C,x} = \langle\tau_{CD,x}\rangle = \tau_{CD,x}\beta_{CD,x}$.[23,24] As shown in Fig. 8, (a) and (b), the relaxation distribution functions could be successfully fitted with the modified Cole–Davidson equation, and the nonlinearly fitted functions were well divided into two characteristic relaxation functions to provide the average relaxation times for the corresponding block domains.

The resulting correlation times of the SIS triblock copolymer and its homopolymer mixtures are shown in Fig. 8, (c) and (d), as a function of temperature. Below ~140 °C (*i.e.*, in the early stages of microphase separation), the molecular motions of PS-rich domains in block copolymer mixtures were faster than those in neat SIS triblock copolymer due to the additional molecular motions of the PS homopolymer molecules diffusing from the PI matrix to the PS domain, induced by the attractive intermolecular affinity between the homologous polymer pair. Around the annealing temperature of 130 °C, the PS-rich domains in perpendicular cylinder-forming SIS + PS12k and SIS + PS15k displayed relatively faster molecular mobility in comparison to the case of parallel cylinder-forming SIS + PS4k, in spite of the larger molecular weights of their homopolymers. We believe that this faster molecular mobility is due to the much stronger homologous PS pair interactions. On the other hand, the molecular mobility of the PS-rich domain in SIS + PS27k was similar to that in SIS + PS4k due to the much higher molecular weight of its homopolymer as well as the significantly reduced homologous PS pair interaction in comparison to the cases of SIS + PS12k and SIS + PS15k. In the early stages of microphase separation, the molecular motions of the PS-rich domain in SIS + PS12k were much faster than those in SIS + PS27k due to its relatively stronger homologous PS pair interaction as well as the significantly lower molecular weight of PS12k. Furthermore, the molecular mobility of the PS-rich domain in SIS + PS12k was even faster than that in SIS + PS15k in spite of its somewhat weaker intermolecular affinity between the homologous PS pair, owing to the lower molecular weight of PS12k. Since fast molecular motions in PS-rich domains represent a large amount of PS homopolymer influx from the PI matrix to the PS domain at a high diffusion rate, the size and center-to-center distance of perpendicular cylinders will increase by increasing the molecular mobility of the PS-rich domain. Recall that the experimental results on the order of size and center-to-center distance of perpendicular cylinders were SIS + PS12k, SIS + PS15k and SIS + PS27k from large to small. However, it is also notable that the perpendicular cylinders have a tendency to lose their hexagonal lattice ordering in the x,y-plane when the molecular motion of the PS domain is too fast as in the case of SIS + PS12k annealed at 130 °C. At the same annealing temperature, on the other hand, the hexagonal orders of perpendicular cylinders in SIS + PS15k were greatly enhanced since the homologous PS pair interaction-induced fast diffusive molecular motions were effectively slowed down by virtue of the molecular weight of PS15k, which was somewhat larger than that of the PS block in the SIS triblock copolymer. As long as the molecular weight ratio of the homologous PS pair is lower than ~2, therefore, we conclude that the blending of a homopolymer with a relatively higher molecular weight in comparison to its corresponding block component is kinetically desirable for the fabrication of hexagonally well-aligned perpendicular cylinders, and the blending of homopolymer with a relatively lower molecular weight is kinetically suitable for enlarging the size of perpendicular cylinders with little loss of their hexagonal lattice alignments.

In further higher temperature regions, the molecular mobility of a block copolymer will be mainly governed by its temperature-dependent morphological transition since its nanostructure growth and ordering processes are coming to an end, and hence there is little influx of PS homopolymer molecules into the PS domains. In this temperature region, therefore, we can evaluate the block copolymer kinetics related to the temperature-dependent block copolymer microphase transition, by comparing the temperature-dependent molecular mobility of a block copolymer with its corresponding microphase transition already described in the previous section. The parallel cylinder-forming SIS + PS4k displayed nearly constant molecular mobility during the parallel cylinder straightening process before its order–disorder transition (ODT) temperature. After the straightening steps, its PS-rich domains showed a sudden increase in molecular mobility near the ODT temperature due to direct phase transition to homogeneous melt states without experiencing any notable inhomogeneous disordering processes of parallel cylinders. The absence of inhomogeneous disordering process in SIS + PS4k suggests that its homopolymer blending-induced segregation forces between the block domains should be negligible, and hence we expect that the actual domain–domain incompatibility of SIS + PS4k is nearly identical to the incompatibility predicted by Flory–Huggins theory.

In the case of perpendicular cylinder-forming SIS + PS12k, the PS-rich domains displayed a dramatic decrease in molecular mobility during the orientation transition process from perpendicular to parallel since the strong intermolecular interactions between the PS homologous pair slowed down such a global phase transition process. After the slow perpendicular to parallel cylinder orientation transition process (*i.e.*, above ~210 °C), the molecular mobility of the PS-rich domains in SIS + PS12k more steadily increased by increasing the temperature in comparison to the cases of parallel cylinder-forming SIS + PS4k. This was due to the continuous phase transition from inhomogeneous disorder states to homogeneous melt states, which originated from the strong segregation force between the block domains (*i.e.*, the strong intermolecular affinity between the homologous PS pair).

Similar to the case of SIS + PS12k, the SIS + PS15k also showed a dramatic decrease of molecular mobility during the merging and lattice disordering process of perpendicular cylinders, and a gradual increase of molecular mobility during the inhomogeneous disordering process, due to the strong intermolecular interactions between the homologous PS pair. In comparison to the case of SIS + PS12k, however, the PS-rich domains in SIS + PS15k displayed: (1) a somewhat slower molecular mobility during the microphase separation process of PS molecules due to the increased molecular weight of blended homopolymer, (2) a little faster molecular mobility during the

merging and lattice disordering process, since a relatively shorter range of molecular motions would be involved in this process, and (3) a somewhat delayed inhomogeneous disordering process due to the relatively stronger intermolecular interaction between the homologous PS pair.

In the case of perpendicular cylinder-forming SIS + PS27k, a relatively slow diffusive molecular mobility was observed in the PS-rich domain at the early stage of microphase separation in comparison to the other perpendicular cylinder-forming block copolymer mixtures, due to: (1) the relatively weak intermolecular interaction between the homologous PS pair (originating from the large molecular weight difference between the homologous PS pair), and (2) the relatively large molecular weight of the blended homopolymer. Similar to the case of SIS + PS12k, the SIS + PS27k also displayed a dramatic decrease in molecular mobility during the perpendicular to parallel cylinder orientation transition process, and a gradual increase in molecular mobility during the inhomogeneous disordering process, due to the still sufficiently strong intermolecular interactions between the homologous PS pair. In comparison to the case of SIS + PS12k, however, the disordering process of SIS + PS27k started to occur at much lower temperatures due to the relatively weaker intermolecular affinity.

From the simple Arrhenius-type dependence of the PI-rich domain molecular mobility on temperature, we can estimate the relative amount of PS molecules present in the PI-rich domain. Since the PS homopolymer constrained in the PI matrix will enlarge the average free volume of PI domains due to the intrinsic repulsive interactions between the two components, the molecular motions in the PI-rich domains will increase as the amount of PS homopolymer trapped in the PI domains increases. Thus, the relative residual amount of PS homopolymer in the PI domain, which inversely correlates with the amount of PS homopolymer diffusing into the PS-rich domain and hence suggests the strength of attractive interactions between the homologous PS pair, can be estimated by comparing the PI-rich domain molecular mobility of the block copolymers used. As shown in Fig. 8 (d), the neat SIS displayed the slowest molecular mobility in its PI-rich domain due to the absence of PS homopolymer molecules in its PI-rich domain. In cases of block copolymer mixtures, the residual amount of PS homopolymer in the PI domain decreased with the increasing strength of intermolecular interaction between the homologous PS pair (*i.e.*, with decreasing molecular weight ratio between the PS homopolymer and its corresponding block in the block copolymer). Thus, the order of slow molecular motions in the PI-rich domain is identical to that of the strong homologous PS pair interaction, *i.e.*, SIS + PS15k, SIS + PS12k, SIS + PS27k and SIS + PS4k.

G. Manipulation of block copolymer self-assembly by controlling the block copolymer thermodynamics and kinetics

Until now, we have considered the kinetic aspects of a block copolymer and its homopolymer mixtures, which correlated with their thermodynamic characteristics. The parallel or perpendicular cylinder orientation of block copolymer mixtures was controlled by the thermodynamic adjustment of the intermolecular affinity between the homologous polymer pair. Furthermore, the size and center-to-center distance of the block copolymer cylinders as well as their hexagonal alignments in the x,y-plane was manipulated by the kinetic control of diffusive molecular mobility between the block domains. We note that such thermodynamic and kinetic aspects involved in the microphase separation processes of block copolymer mixtures provide a critical theoretical basis required for further precise controls of block copolymer microstructures. As an example, the PS12k can be utilized as a 'kinetic modifier' controlling the size of perpendicular cylinders in SIS + PS15k and SIS + PS27k, and at the same time it can be used as a 'thermodynamic modifier' enhancing the preference for perpendicular cylinder orientation in SIS + PS27k.

As shown in Fig. 9, the size and center-to-center spacing of perpendicular cylinders in SIS + PS12k + PS15k linearly increased with increasing amounts of PS12k because the additionally incorporated PS12k enhanced the diffusive molecular mobility of PS15k. The hexagonal orders of perpendicular cylinders in SIS + PS12k + PS15k did not notably decrease even at 7 wt% of PS12k (see the 2D FFTs included as insets in Fig. 9) since the small amount of PS15k effectively suppressed the over-acceleration effects of PS12k. Similarly, the size and center-to-center spacing of perpendicular cylinders in SIS + PS12k + PS27k also linearly increased with increasing amounts of PS12k, and the perpendicular cylinders maintained their hexagonal orders even at 9 wt% of PS12k (Fig. 10). It is also notable that the SIS + PS12k + PS27ks containing more than 5 wt% of PS12k did not show a thickness-dependent orientation transition up to a thickness of ~10 μm due to the increase of intermolecular interaction between the homologous PSs as well as the decrease in immiscibility between the SIS and PS27k, after the additional blending of the 'thermodynamic modifier', PS12k. Consequently,

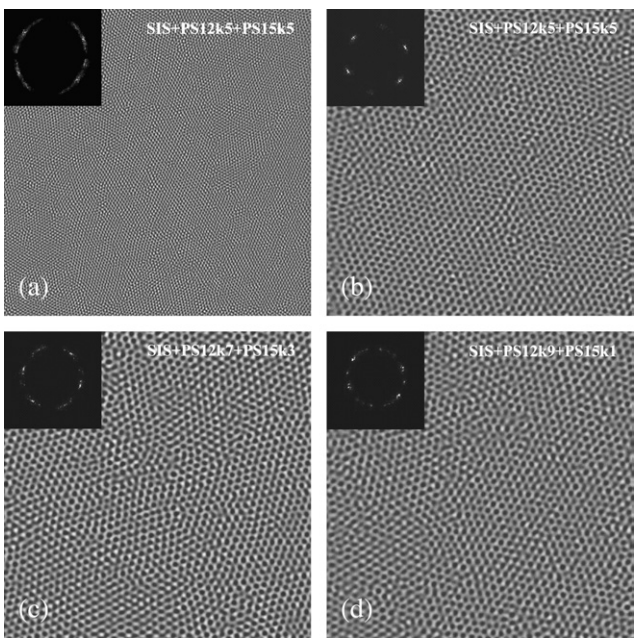

Fig. 9 AFM images of SIS + PS12k + PS15k's. Images were obtained from ~10 μm thick samples annealed at 130 °C on the Teflon substrates. Topographic and phase AFM images were the same. The inset of the AFM image is a 2D FFT of the image. The images show areas of 5 × 5 μm^2 (a) or 2 × 2 μm^2 (b, c, and d).

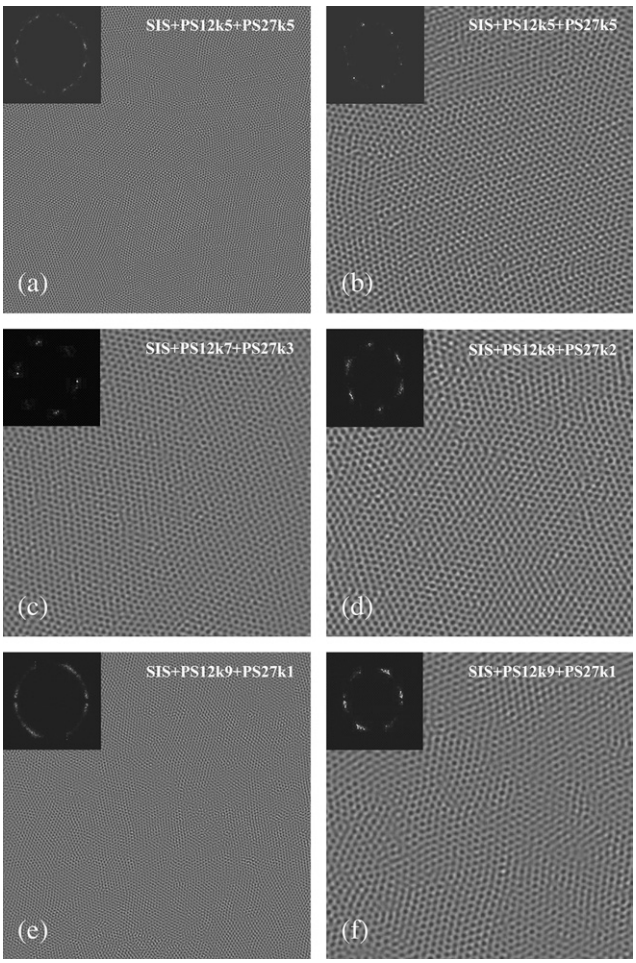

Fig. 10 AFM images of SIS + PS12k + PS27ks. Images were obtained from ~10 μm thick samples annealed at 130 °C on the Teflon substrates. Topographic and phase AFM images were the same. The inset of the AFM image is a 2D FFT of the image. The images show areas of 5 × 5 μm^2 (a and e) or 2 × 2 μm^2 (b, c, d, and f).

the perpendicular cylinder-forming block copolymer mixture, SIS + PS12k + PS27k provided a wide-range of cylinder diameters from ~25 to ~35 nm by increasing the ratio of PS12k without micrometre-scale macrophase separation between the SIS and PS27k as long as the sample thickness was lower than ~10 μm.

IV. Conclusions

In summary, we have prepared well-aligned 3-dimensional block copolymer nano-cylinders over the entire sample area and thickness without any application of external fields such as electric and flow fields. Based on the experimental results providing self-assembled block copolymer nano-cylinders with perpendicular and hexagonal alignments on a preferential substrate without any external field applications, we demonstrated the presence of enthalpic intermolecular interaction between the homologous polymer pair. Straightness-controllable block copolymer cylinders with parallel orientation were produced within a relatively weak homologous polymer pair interaction limit. In comparison, self-assembled perpendicular cylinder orientation was achieved within a relatively strong homologous polymer pair interaction limit, mainly by thermodynamic controls of intermolecular interaction between the homologous polymer pair. Further precise modifications of size and hexagonal alignment of perpendicular cylinders were also accomplished by kinetic control of diffusive molecular mobility of block copolymer microdomains. From the viewpoint of nanotechnology using block copolymer nanopatterns, we believe our proposed fabrication methods based on the thermodynamics and kinetics of block copolymer self-assembly will provide the basic guidelines required for the fabrication of nanoscopically well-defined block copolymer materials.

References

1 T. L. Morkved, M. Lu, A. M. Urbas, E. E. Ehrichs, H. M. Jaeger, P. Mansky and T. P. Russell, *Science*, 1996, **273**, 931.
2 M. Park, C. K. Harrison, P. M. Chaikin, R. A. Register and D. H. Adamson, *Science*, 1997, **276**, 1401.
3 C. Park, J. Yoon and E. L. Thomas, *Polymer*, 2003, **44**, 6725.
4 C. C. Honeker and E. L. Thomas, *Chem. Mater.*, 1996, **8**, 1702.
5 Z. Chen, J. A. Kornfield, S. D. Smith, J. T. Grothaus and M. M. Satkowski, *Science*, 1997, **277**, 1248.
6 H. Kim, X. Jia, C. M. Stafford, D. H. Kim, T. J. McCarthy, M. Tuominen, C. J. Hawker and T. P. Russell, *Adv. Mater.*, 2001, **13**, 795.
7 G. Kim and M. Libera, *Macromolecules*, 1998, **31**, 2569.
8 H. Li and W. T. S. Huck, *Nano Lett.*, 2004, **4**, 1633.
9 U. Jeong, D. Y. Ryu, D. H. Kho, J. K. Kim, J. T. Goldbach, D. H. Kim and T. P. Russell, *Adv. Mater.*, 2004, **16**, 533.
10 D. U. Ahn and E. Sancaktar, *Adv. Funct. Mater.*, 2006, **16**, 1950. Further details on the perpendicular cylinder orientation of the block copolymer mixtures throughout the whole sample thickness are available in the ESI†.
11 T. Hashimoto, H. Tanaka and H. Hasegawa, *Macromolecules*, 1990, **23**, 4378.
12 K. I. Winey, E. L. Thomas and L. J. Fetters, *Macromolecules*, 1992, **25**, 2645.
13 S. H. Lee, K. Char and G. Kim, *Macromolecules*, 2000, **33**, 7072.
14 T. A. Mykhaylyk, O. O. Mykhaylyk, S. Collins and I. W. Hamley, *Macromolecules*, 2004, **37**, 3369.
15 M. P. Stoykovich, M. Müller, S. O. Kim, H. H. Solak, E. W. Edwards, J. dePablo and P. F. Nealey, *Science*, 2005, **308**, 1442.
16 I. W. Hamley, *The Physics of Block Copolymers*, Oxford University Press, NY, 1998.
17 C. D. Han, D. M. Baek, J. K. Kim, T. Ogawa, N. Sakamoto and T. Hashimoto, *Macromolecules*, 1995, **28**, 5043.
18 Further details on the thermodynamic and kinetic stability of the block copolymers are available in the ESI†.
19 S. Wu, *Polymer Interface and Adhesion*, Marcel Dekker Inc., New York, 1982.
20 E. Huang, L. Rockford, T. P. Russell, C. J. Hawker and J. Mays, *Nature*, 1998, **395**, 757.
21 K. Y. Suh, Y. S. Kim and H. H. Lee, *J. Chem. Phys.*, 1998, **108**, 1253.
22 G. Szamel and M. Müller, *J. Chem. Phys.*, 2003, **118**, 905.
23 C. P. Lindsey and G. D. Patterson, *J. Chem. Phys.*, 1980, **73**, 3348.
24 S. Kwak and D. U. Ahn, *Macromolecules*, 2000, **33**, 7557.
25 S. Kwak, D. U. Ahn, J. Choi, H. J. Song and S. Lee, *Polymer*, 2004, **45**, 6889.
26 S. Matsuoka, *Relaxation Phenomena in Polymers*, Hanser, NY, 1992.
27 D. W. Davidson and R. H. Cole, *J. Chem. Phys.*, 1950, **18**, 1417.
28 D. W. Davidson and R. H. Cole, *J. Chem. Phys.*, 1951, **19**, 1484.
29 M. C. Dalvi, C. E. Eastman and T. P. Lodge, *Phys. Rev. Lett.*, 1993, **71**, 2591.
30 J. D. Ferry, *Viscoelastic Properties of Polymers*, John Wiley & Sons Inc., NY, 1980.
31 (1) Thermal histories of neat SIS annealed at 150 °C: first annealed at 130 °C for 47.5 h and then heated to 150 °C and held there for 2.5 h and then rapidly quenched in liquid nitrogen. (2) Thermal histories of SIS + PS4k, SIS + PS12k, SIS + PS15k and SIS + PS27k annealed at 170 °C: first annealed at 130 °C for 47.5 h and then heated to 150 °C

and held there for 1 h and then heated to 170 °C and held there for 0.5 h and then rapidly quenched in liquid nitrogen. (3) Thermal histories of SIS + PS12k and SIS + PS15k annealed at 210 °C: first annealed at 130 °C for 47.5 h and then heated to 150 °C and held there for 1 h and then heated to 170 °C and held there for 0.5 h and then heated to 190 °C and held there for 0.5 h and then heated to 210 °C and held there for 0.5 h and then rapidly quenched in liquid nitrogen. (4) Thermal histories of SIS + PS27k annealed at 190 °C: first annealed at 130 °C for 47.5 h and then heated to 150 °C and held there for 1 h and then heated to 170 °C and held there for 0.5 h and then heated to 190 °C and held there for 0.5 h and then rapidly quenched in liquid nitrogen.